

## Article

# Effect of Nanovoid on Fracture Process of Two-Phase $\gamma(\text{TiAl})+\alpha(\text{Ti}_3\text{Al})$ Alloy

Firstname Lastname<sup>1,t,‡</sup>, Firstname Lastname<sup>1,‡</sup> and Firstname Lastname<sup>2,\*</sup>

<sup>1</sup> School of Mechanical and Electronical Engineering, Lanzhou University of Technology, Lanzhou 730050, China; e-mail@e-mail.com

<sup>2</sup> Affiliation 2; e-mail@e-mail.com

\* Correspondence: e-mail@e-mail.com; Tel.: +x-xxx-xxx-xxxx

† Current address: Affiliation 3

‡ These authors contributed equally to this work.

Version September 27, 2018 submitted to Journal Not Specified

**Abstract:** Fracture processes of nanocrystalline metallic materia is affected by dislocation, nanovoid and other defects. Existing studies of defect evolution in titanium-aluminium alloy cover the case that voids located in single crystals, inside grain in poly crystals and at the grain boundaries. Molecular dynamics simulation was performed to study the evolution of a spherical nanovoid in  $\alpha+\gamma$  two-phase titanium-aluminium alloy under uniaxial tension. The results show that voids located at the  $\alpha/\gamma$  phase boundary have significant detract to strength of Ti-Al polycrystalline.

**Keywords:**  $\alpha + \gamma$  two phase TiAl alloy; void; molecular dynamics

## 1. Introduction

### Material

TiAl alloy has been used as structural material in aviation industry because its inherent advantages such as low density and self-diffusion rates, high elastic module and high strength [1]. Two-phase titanium aluminum alloys with proper phase distribution and grain size exhibit better mechanical performance compared with monolithic constituents  $\gamma(\text{TiAl})$  and  $\gamma(\text{Ti}_3\text{Al})$  alloy [2]. Brittle fracture in TiAl alloy strongly affects the safety of fracture of structure like turbo of aircraft engine and combustion generator.

The failure modes of materials have significant influence on the design of material properties in materials science. Rapture failure at the macroscopic scale can be attributed to nucleation, growth and propagation of cracks, but at the microscopic scale cracks are initially easily formed at defects in the casting process, such as voids and inclusions [3]. These defects are known to play a fundamental role in the deformation of the material. Nucleation, growth and coalescence of voids are deemed as the primary mechanism of ductile material fracture, in which void growth is particularly important. Therefore, it is necessary to study the deformation response of porous materials with the consideration of microstructure evolution.

Brittle fracture in TiAl alloy strongly affects the safety of fracture of structure like turbo of aircraft engine and combustion generator [4]. Defects such as grainboundary, void and segregation plays an significant role in the process of fracture [5]. In order to understanding the mechanism of brittle fracture, multi-scale methods from micro to marco scale have been applied to investigate the behavior of fracture. It's necessary to carefully examine the revolution of defects and its influence on the fracture process at atomic scale. A previous study on void growth in gamma-TiAl single crystal has reveals that void with high volume fraction detracts incipient yield strength [6]. Molecular dynamics(MD) method

<sup>31</sup> has been used to investigate the evolution of void in materials in nanoscale [ ]. The fracture mechanisms  
<sup>32</sup> in the duplex micro-structure are plasticity induced grain boundary decohesion and cleavage, while  
<sup>33</sup> those in the lamellar microstructure are interface delamination and cracking across the lamellae [ ].

## <sup>34</sup> 2. Molecular Dynamics Simulation

### <sup>35</sup> 2.1. Atomic Potential

<sup>36</sup> The interaction of particle in the material is determined by interatomic potential. Many reported  
<sup>37</sup> examples of crack propagation in metal materials were performed with embedded atomic method  
<sup>38</sup> due to its better accuracy in metal lattice compare with F-S and L/J [ ]. The embedded atom method  
<sup>39</sup> (MEAM) potential developed by Zope and Mishin by [ ] was used in the study. The simulation is  
<sup>40</sup> submitted by MD simulations with the Large-scale Atomic/Molecular Massively Parallel Simulator  
<sup>41</sup> (LAMMPS) open-source code [ ]. We performed constant-pressure and constant-temperature (NPT)  
<sup>42</sup> molecular dynamics simulation.

$$E_{total} = \sum F_i(\rho_{h,i}) + \frac{1}{2} \sum_i \sum_{j(\neq i)} \phi_{ij}(R_{ij}) \quad (1)$$

<sup>43</sup> where  $E_{total}$  is the total energy of the system,  $\rho_{h,i}$ , is the host electron density at atom  $i$  due to the  
<sup>44</sup> remaining atoms of the system,  $F_i(\rho)$  is the energy for embedding atom  $i$  into the background electron  
<sup>45</sup> density  $\rho$ , and  $\phi_{ij}(R_{ij})$  is the core-core pair repulsion between atoms  $i$  and  $j$  separated by the distance  
<sup>46</sup>  $R_{ij}$ . It can be noted that  $F_i$  only depends on the element of atom  $i$  and  $\phi_{ij}$  only depends on the elements  
<sup>47</sup> of atoms  $i$  and  $j$ . The electron density is, as stated above, approximated by the superposition of atomic  
<sup>48</sup> densities, namely

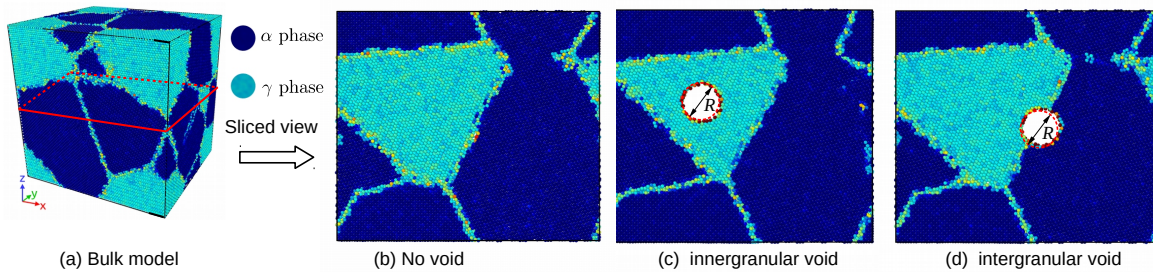
$$\rho_{h,i} = \sum_{j(\neq i)} \rho_i(R_{ij}) \quad (2)$$

### <sup>49</sup> 2.2. Model Creation of Crystalline

<sup>50</sup>  $\gamma$  TiAl has a fcc-centered tetragonal with an  $L1_0$  structure [ ], and  $\alpha$ TiAl is hcp structure, the  
<sup>51</sup> structure of the two initial cells are shown in Fig. [ ], and the constructing parameters are given by Table. [ ].  
<sup>52</sup> The simulation cells of two phase polycrystalline with an initially spherical void at different position  
<sup>53</sup> are shown in figure [ ]. Periodic boundary conditions (PBC) are applied along all three directions, that  
<sup>54</sup> makes poly crystal with periodic nanovoid structures. The initial dimension of simulation cell is  $L_x =$   
<sup>55</sup> nm,  $L_y =$  nm,  $L_z =$  nm, and each model contains about 4.6 million atoms. The grain orientation and  
<sup>56</sup> size were randomly created with Voronoi method with code ATOMSK [ ], and resulting in the arbitrary  
<sup>57</sup> shape and orientation of the grains. Only one spherical void defect was placed intragranularly or  
<sup>58</sup> intergranularly within each simulation model void within each simulation model. The intragranular  
<sup>59</sup> spherical void was located in grain interior of the largest grain of the simulation model, as shown in  
<sup>60</sup> Fig. [ ]. The intergranular spherical void was at the center of the simulation cell, as shown in Fig. [ ].

**Table 1.** Parameters of nanocrystalline

Phase	Space group	Designation	Parameters
$\alpha_2$	P6 <sub>3</sub> /mmc	$0_{19}$	$a = 0.5765$ $c = 0.46833$
$\gamma$	tP4	$L1_0$	$a = 0.3997$ $c = 0.4062$

**Figure 1.** Overview of model creation

**61** *2.3. Analysis method*

**62** **CSP**

The centrosymmetry parameter is defined as follow:

$$P = \sum_{i=1}^6 |\vec{R}_i + \vec{R}_{i+6}|^2 \quad (3)$$

**63** where  $\vec{R}_i$  and  $\vec{R}_{i+6}$  are the vectors corresponding to the six pairs of opposite nearest neighbors  
**64** in the fcc lattice. The centrosymmetry parameter(CSP) is zero for atoms in a perfect lattice. In other  
**65** words, if the lattice is distorted the value of P will not be zero. Instead, the parameter will have a value  
**66** within the range corresponding to a particular defect. By removing all the perfect and surface atoms  
**67** within the bulk, the existence of dislocation atoms become visible.

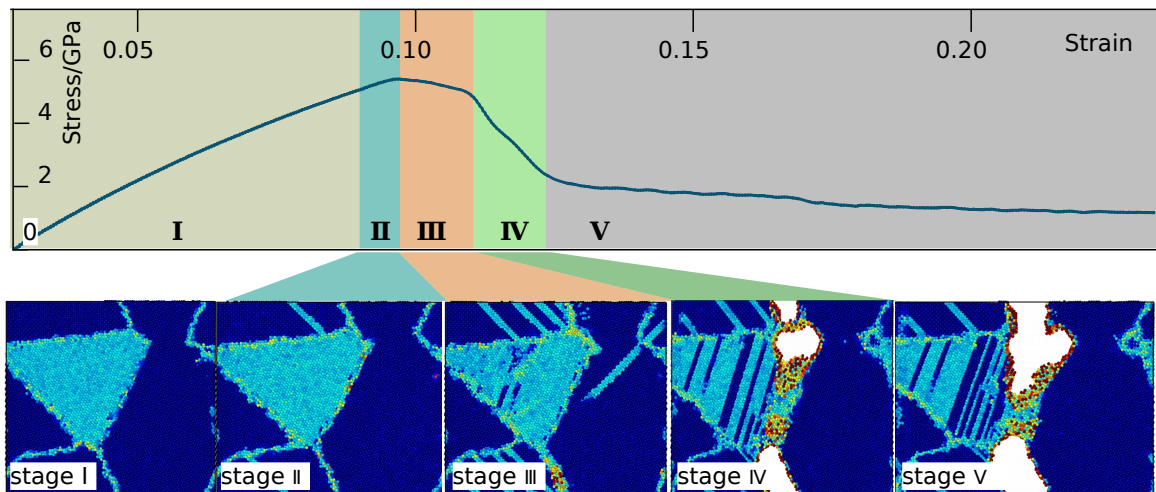
**68** **Virial Stress**

The atomic stress is calculated using the virial definition :

$$\sigma_t(i) = -$$

$$\sigma_t(i) =$$

**69** **3. Results and Discussion**

**Figure 2.** perfect-line2-2

70 *3.1. Deformation Mechanisms in Two-Phase Alloys*

71 Deformation phenomena in TiAl alloys have been widely studied in order to overcome the  
 72 problems associated with the limited ductility and damage tolerance. The literature data covers a wide  
 73 range of parameters such as alloy composition, microstructure and deformation temperature. Much  
 74 of the work has been performed on single phase  $\gamma$  alloys and PST crystals. However, the following  
 75 discussion concentrates on deformation phenomena that rely on the elastoplastic codeformation of the  
 76  $\gamma$  and  $\gamma_2$  phases and on the particular point defect situation occurring in twophase alloys. Due to this  
 77 effect ( $\alpha_2 + \gamma$ ) alloys exhibit some remarkable properties that are unlike those of either constituent.  
 The configue of atoms is shown in Fig.5, it can be seen that dislocation emission initiate in  $\gamma$  pahse

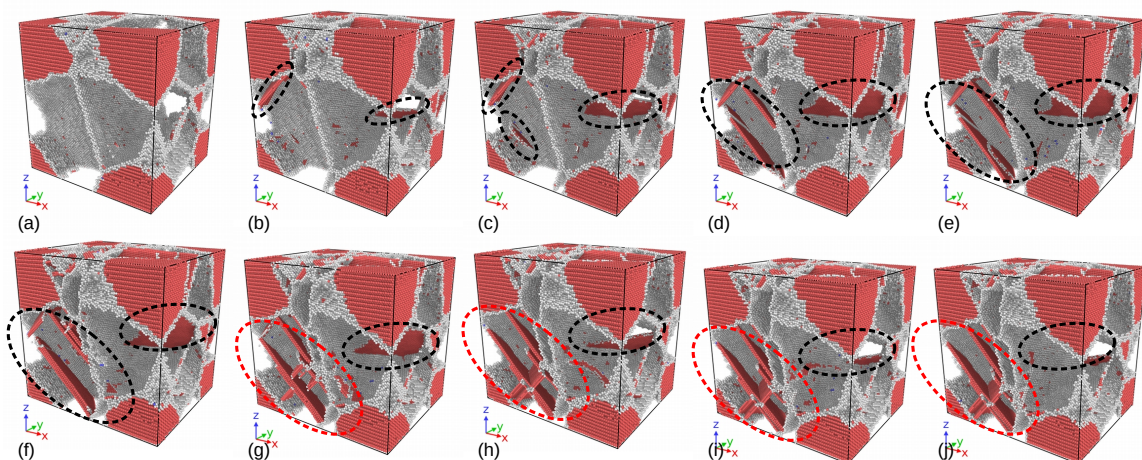


Figure 3.  $\gamma$  phase deformation

78 in XXX ps, and the deformation canbe mainly confied to the majority  $\gamma$  pahse.  $\gamma$ (TiAl) deforms by  
 79 octahedral glide of ordinary dislocations with the Burgers vector  $b=1/2<110]$  and superdislocations  
 80 with the Burgers vectors  $b=<101]$  and  $b = 1/2 < 11\bar{2}]$ . The other potential deformation mode is  
 81 mechanical twinning along  $1/6 < 11\bar{2}]111$ . From Fig.5, of the two constituents of ( $\alpha_2+\gamma$ ) alloys, the  
 82  $\alpha_2$  phase is more difficult to deform. A reason for the unequal strain partitioning between the  $\alpha_2$  and  
 83  $\gamma$  phase is certainly the strong plastic anisotropy of the  $\alpha_2$  phase. TEM examinations performed on  
 84 tensile tested lamellar alloys have revealed that the limited plasticity of the  $\alpha_2$  phase is mainly carried  
 85 by local slip of  $<\mathbf{a}>$ -type dislocations with the Burgers vector  $b = 1/3 < 11\bar{2}0 >$  prism planes<sup>5</sup>, which  
 86 is by far the easiest slip system in  $\alpha_2$  single crystals. Basic deformationg mechanism of  $\alpha$  phase

87 1.In many cases the orientation of slip slip is changed because the crystallographically available  
 88 slip and directions are not continuous across the interface. This may significantly reduce the Schmid  
 89 factor and thus impede slip transfer. At the  $\gamma/\gamma$  interfaces the orientation of the slip plan could change  
 90 through a relevantly large angle of about 90 degree. Reorientation of slip is always required at the  
 91  $\alpha_2/\gamma$  interface; the smallest angle between the corresponding slip planes  $111_\gamma$  and  $10 - 10_{\alpha_2}$  is about  
 92 19 degree [].

93 The core of a dislocation intersecting an interface often needs to be transformed. For example, an  
 94 ordinary  $1/2<110]$  dislocation gliding in one  $\gamma$  grain has to be converted in to a  $<101]$  super dislocation  
 95 with the double Burgers vector gliding in an adjacent  $\gamma$  grain. At the  $\alpha/\gamma$  interface the dislocations  
 96 existing in the  $D0_{19}$  structure have to be transformed into dislocations consistent with the  $L1_0$ structure.  
 97 These core transformations are associated with a change of the dislocation line energy because the  
 98 lengths of the Burgers vectors and the shear module are different.

99 Dislocations crossing semi-coherent boundaries have to intersect the misfit dislocations, a process  
 100 that involves elastic interaction, jog formation and the incorporation of gliding dislocations into the

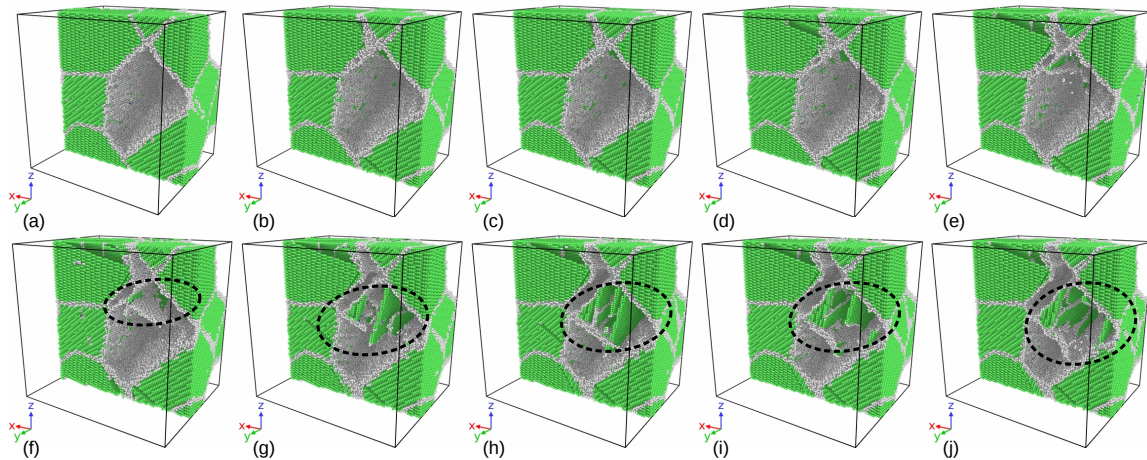


**Figure 4.**  $\alpha$  phase deformation

102 mismatch structure of the interface. When the slip is forced to cross  $\alpha_2$  lamella, pyramidal slip of the  $\alpha_2$   
103 phase is required, which needs an extremely high shear stress.

104 *3.2. Evolution of spherical void in the simulation with intragranular spherical voids*

105 A step, of the width of a burgers vector, will be generated at both sidesof a crystal along teh  
106 direction of teh burgers vector after dislocation traversing teh entire crystal, as is shown in ???. A small  
107 tep will be formed at spherical void surface toward teh void interiorafter dislocation absorbtionat  
108 sphericalvoid surfaces, as is shown in ???. If a great number of dislocation slip along their respective  
109 systemstowards teh spherical nanovoid in all directions, and are absorbed at spherical void surfaces,  
110 the spherical nanovoid will eventually shrink from teh dash circle to

111 *3.3. The effect of void on the strength of material*

112 position

113 Void of R=10 was placed at phase boundary, inside  $\alpha$  phase grain respectively. Effect of void at  
114 different position under uniaxial tension is shown in Fig.8. The strength of materails with void in  
115 different size and at different position is shown in Fig.8. The results show that the model without void  
116 defect has best stength, while the void loacted inside  $\alpha$  phase detracts the strength of the material most,  
117 and the void at the phase boundary have less impact on the strength.

118 size

119 The effect of siz is expectable that the greater voids detracts the strength of the materials more,  
120 however, it has been observed in the simulation that there is a critical value about 15A for voids at  
121 different position. The voids larger than 15 A have dramatic detraction to the strength of the material.  
122 Conventional definition of strength of materails with geometry subtraction was applied to the model,  
123 and therotcial strength of the models was calculated by formulation 4:

$$\sigma^* = \sigma_0 \cdot \frac{A^*}{A_0} \quad (4)$$

124 where  $\sigma_0$  is the strength of the model without void defects 5.26 Gpa, and  $A_0$  is initial section area,  
125  $A = a \times b = 36000A^2$ ,  $A^*$  is section area in consider of the subsection that results from the voids.  
126 Comparing with the strength determined by molecular dynamics simulation and the results calculated

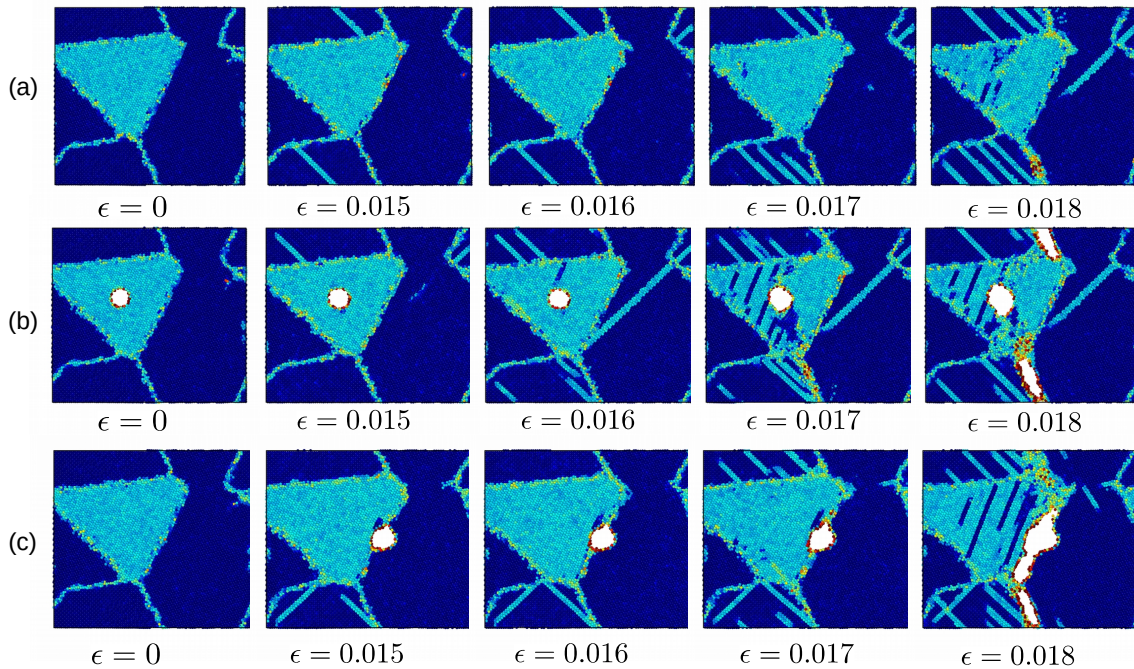


**Figure 5.** Yield process of the models

with formulation 4, it can be assumed that the main factor that affects the strength of materials can be attributed to local behaviour of the materials, thus revolution of defects should be examined carefully.

Voids with different size: 2A, 5A, 10A, 15A were placed into the model respectively. It has been observed that voids detracts the strengths of the material. The max stress stress of the simulation cell decreases as the volume of voids are lareger. From Fig ??, there is a critical value of void radius about 15A, the void greater than 15A cause serious detraction of strength of material. Engineering stress is calculated

$$\sigma = S/A$$

The rate of decrease of loading area are smaller comparing with the detraction of strength, so it can be assumed that the yield yield behaviour and strength is much more related with local behaviour of grain boundaries and void.

Grain and phase boundaris are obstacles to deformation process, thus the stability of boundaries have great impact on the strength of materials. Interactive between grainboundary and void determines the fracture mode of the TiAl alloy.

According to Schmid's law:

$$\tau = \sigma * m$$

where m is the Schmid factor :

$$m = \cos(\phi)\cos(\lambda)$$

135

136 position

137 critical void The location of void affects strength of material. Comparing with the model with  
138 intergranular void, the model with intergranular voids is weaker. atomic stress is calculated

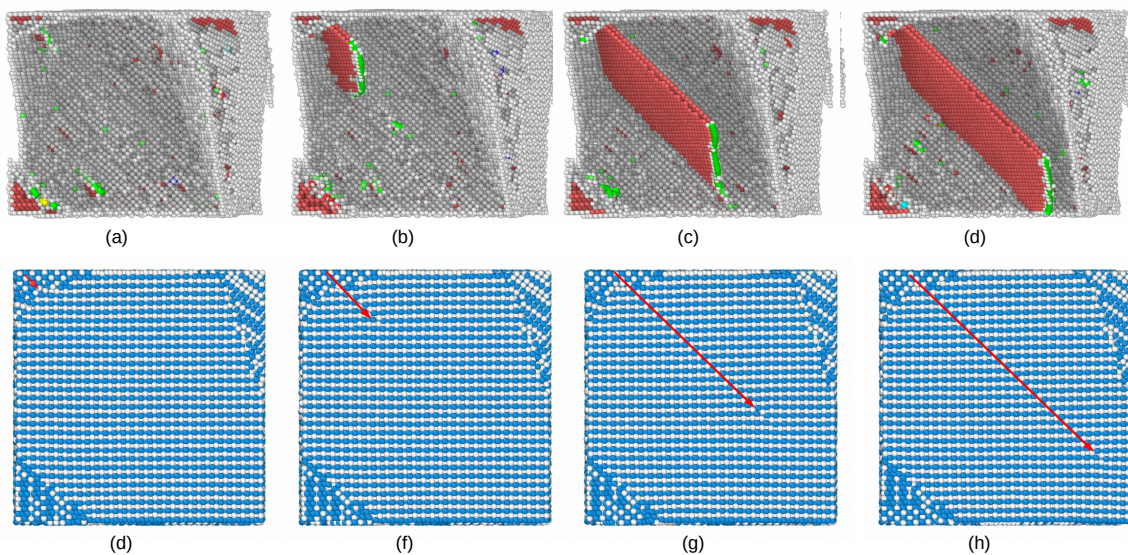


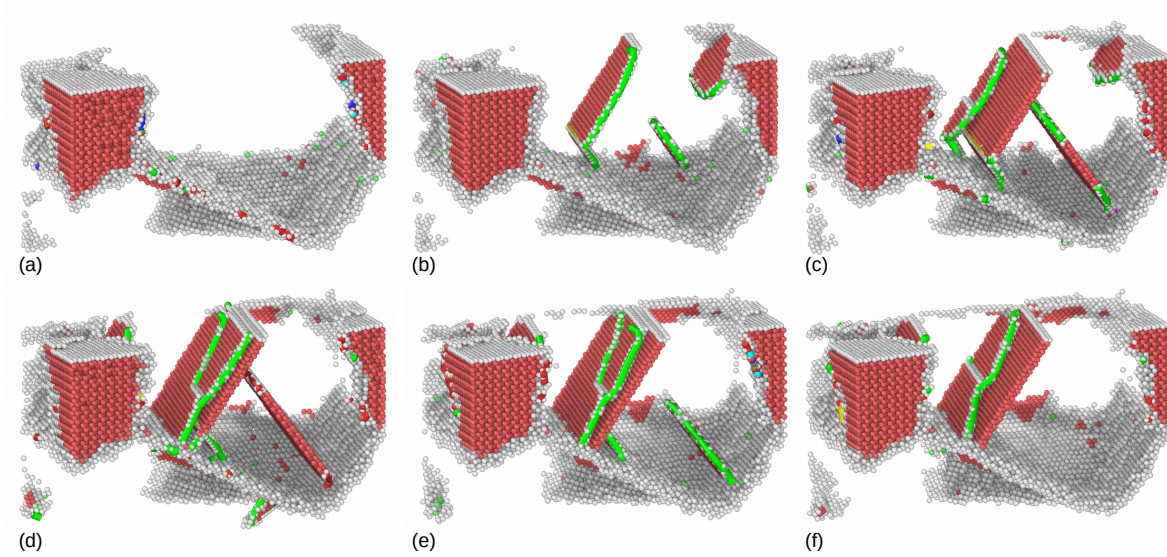
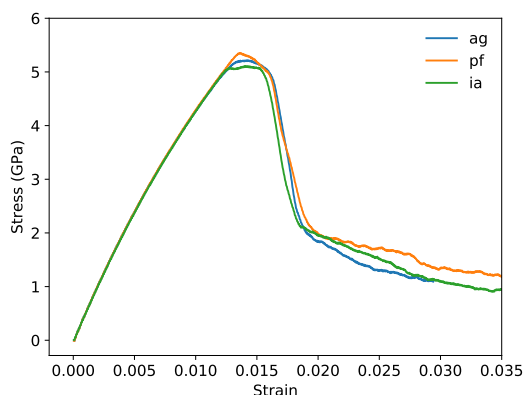
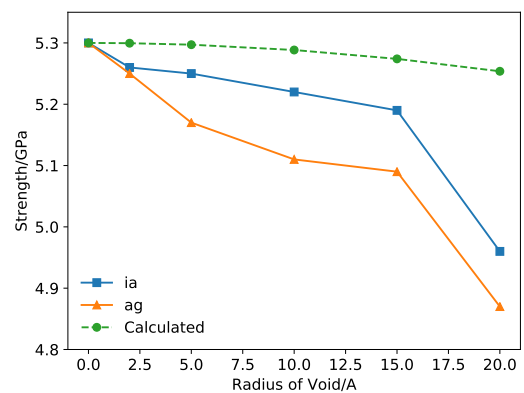
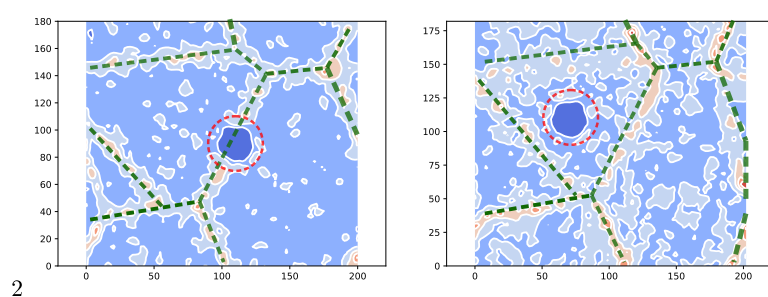
**Figure 6.** Dislocation in  $\gamma$

**139 4. Conclusion**

**140**

- 141** 1. Vu, T.T.T.; Zehender, T.; Verheijen, M.A.; Plissard, S.R.; Immink, G.W.G.; Haverkort, J.E.M.; Bakkers,  
**142** E.P.A.M. High optical quality single crystal phase wurtzite and zincblende InP nanowires. *Nanotechnology*  
**143** **2013**, *24*, 115705. doi:10.1088/0957-4484/24/11/115705.

**144** © 2018 by the authors. Submitted to *Journal Not Specified* for possible open access  
**145** publication under the terms and conditions of the Creative Commons Attribution (CC BY) license  
**146** (<http://creativecommons.org/licenses/by/4.0/>).

**Figure 7.** stress-strain curve**Figure 8.** Stress-Strain**Figure 9.** Strength of models**Figure 10.** stress- $\sigma=0$

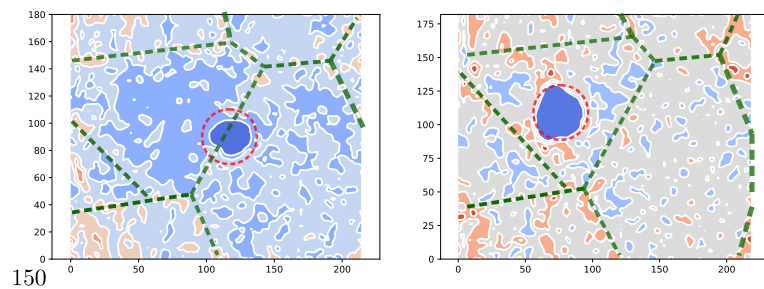


**Figure 11.** stress- $\sigma=0.15$

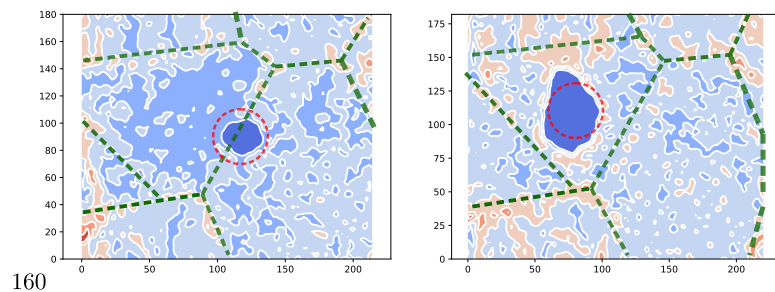


**Figure 12.** stress- $\sigma=0.16$

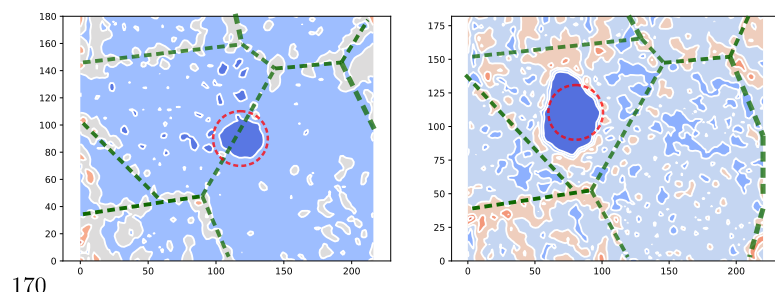


**Figure 13.** stress- $\sigma=0.17$

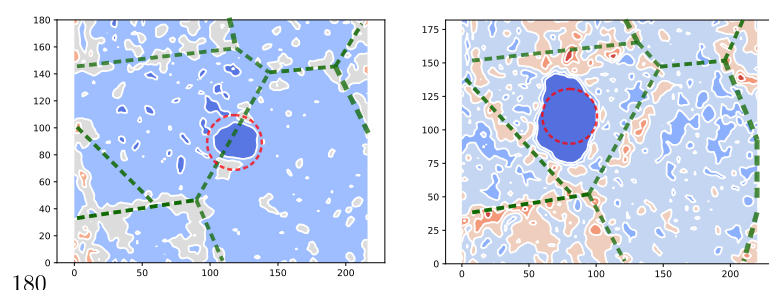


**Figure 14.** stress- $\sigma=0.18$

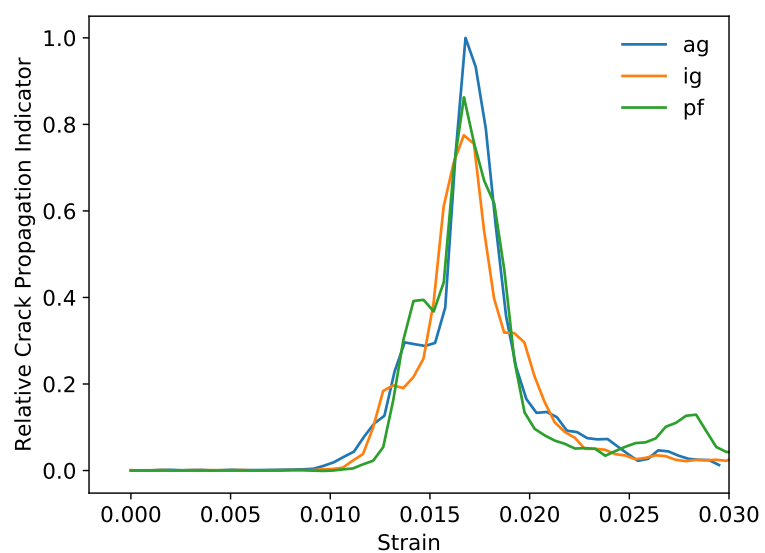


**Figure 15.** stress-strain curve